Chapter 10

Z-Source Inverter for Automotive Applications

Omar Ellabban and Joeri Van Mierlo

Additional information is available at the end of the chapter

http://dx.doi.org/10.5772/52724

1. Introduction

In a context of volatile fuel prices and rising concerns in terms of energy security of supply and climate change issues, one of the discussed technological alternatives for the transportation sector are electric based vehicles. Advanced technology vehicles such as hybrid electric vehicles (HEVs), plug-in hybrid electric vehicles (PHEVs), fuel cell hybrid electric vehicles (FCHEVs), and electric vehicles (EVs) require power electronics and electrical machines to function. These devices allow the vehicle to use energy from the battery to assist in the propulsion of the vehicle, either on their own or in combination with an engine [1]. Therefore, many research efforts have been focused on developing new converters and inverters suitable for electric vehicles applications. One of the most promising topologies is the Z-source inverter (ZSI). The ZSI, as shown in Figure 1, is an emerging topology for power electronics DC/AC converters. It can utilize the shoot-through (ST) state to boost the input voltage, which improves the inverter reliability and enlarges its application field [2]. In comparison with other power electronics converters, it provides an attractive single stage DC/AC conversion with buck-boost capability with reduced cost, reduced volume and higher efficiency due to a lower component number. Therefore, the ZSI is a very promising and competitive topology for vehicular applications [3].

As a research hotspot in power electronics converters, the ZSI topology has been greatly explored from various aspects, such as: ST control methods [2], [4]-[8], designing of the Z-network elements [9], modeling of the ZSI [10], [11], feedback control strategies [12]-[26], motor control algorithms [27]-[31] and automotive applications [32]-[37].

This chapter starts by presenting a summary for ZSI operation modes and modeling. Then, a review and a comparison between four ST boost control methods, which are: simple boost control (SBC), maximum boost control (MBC), maximum constant boost control (MCBC), and modified space vector modulation (MSVM) boost control, is presented based on simulation and experimental results. Control strategies of the ZSI are important issue and several

feedback control strategies have been investigated in recent publications. There are four methods for controlling the dc-link voltage of the ZSI, which are: capacitor voltage control, indirect dc-link voltage control, direct dc-link control and unified control. A review of the above mentioned control methods with their drawbacks will be presented. Two new proposed control methods, which are dual-loop capacitor voltage control and dual-loop peak dc-link voltage control, will be presented and demonstrated by simulation and experimental results. Then, this chapter presents a comparative study of the most significant control methods, which are: scalar control (V/F), indirect field oriented control (IFOC) and direct torque control (DTC), for an induction motor fed by a ZSI for automotive applications. These control techniques are implemented using PWM voltage modulation. Finally, this chapter proposes three applications of the ZSI for automotive applications.

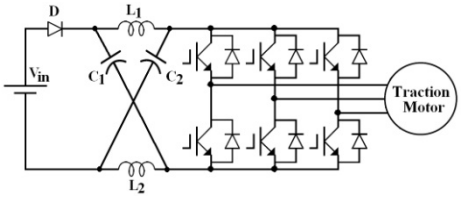

Figure 1. ZSI basic structure

2. ZSI Operation Modes and Modeling

To design a controller for the ZSI, a proper dynamic model for its switching operation is needed. An accurate small signal model of the ZSI gives not only a global also a detailed view of the system dynamics and provides guidelines to system controllers design since the transfer functions could be derived accordingly. Figure 1 shows the basic ZSI topology, which consists of two inductors (L1 and L2) and two capacitors (C1 and C2) connected in X shape to couple the inverter to the dc voltage source. The ZSI can produce any desired ac output voltage regardless of the dc input voltage. Because of this special structure, the ZSI has an additional switching state, when the load terminals are shorted through both the upper and lower switching devices of any phase leg, which called the shoot-through (ST) state besides the eight traditional non-shoot through (NST) states. General operation of a ZSI can be illustrated by simplifying the ac side circuit by an equivalent RL load in parallel with a switch S_2 and the input diode D is represented by a switch S_1, as shown in Figure 2. Where, R_l is given by $R_l = 8 \mid Z_{ac} \mid / 3\cos\phi$ and L_l is determined so that the time constant of the dc load is the same as the ac load [16]. Two operation modes involving two different circuit topologies can be identified in the ZSI operation as shown in Figure 3. In Mode 1, Figure 3-a, the energy transferred from source to load is zero because the load side and source side are decoupled by the ST state and the open status of S1. In Mode 2, Figure 3-b, real energy transfer between source and load occurs.

http://dx.doi.org/10.5772/52724

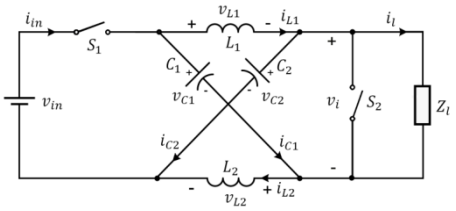

Figure 2. A simplified equivalent circuit for the ZSI

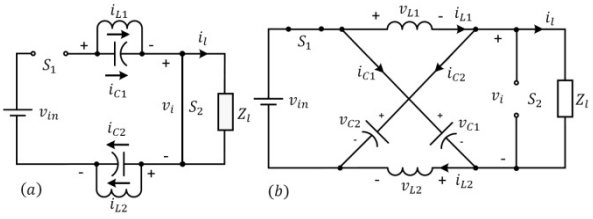

Figure 3. The basic two equivalent operation modes: (a) ST state, (b) NST state

Equations (1-4) represent: the third order small signal model, the steady state values of the state variables, the control to capacitor voltage $G_{vd}(s)$and control to inductor current $G_{id}(s)$ small signal transfer functions of the ZSI, where V_{in}, R_l, L_l, I_L, V_C, I_l, $D_0$are the input voltage, the equivalent dc load resistance, the equivalent dc load inductance, and the steady state values of inductor current, capacitor voltage, load current and ST duty ratio at certain operating point, respectively, and L , $C$are the Z-network inductor and capacitor, respectively.

$$\frac{d}{dt}\begin{bmatrix}\tilde{i}_L(t)\\ \tilde{v}_c(t)\\ \tilde{i}_l(t)\end{bmatrix}=\begin{bmatrix}0 & \frac{2D_0-1}{L} & 0\\ \frac{1-2D_0}{C} & 0 & \frac{-(1-D_0)}{C}\\ 0 & \frac{2(1-D_0)}{L_l} & \frac{-R_l}{L_l}\end{bmatrix}\cdot\begin{bmatrix}\tilde{i}_L(t)\\ \tilde{v}_c(t)\\ \tilde{i}_l(t)\end{bmatrix}+\begin{bmatrix}\frac{1-D_0}{L}\\ 0\\ \frac{-(1-D_o)}{L_l}\end{bmatrix}\cdot\tilde{v}_{in}(t)+\begin{bmatrix}\frac{2V_C-V_{in}}{L}\\ \frac{-2I_L+I_l}{C}\\ \frac{-2V_C+V_{in}}{L_l}\end{bmatrix}\cdot\tilde{d}_0(t) \tag{1}$$

$$\begin{aligned}V_C&=\frac{1-D_o}{1-2D_0}V_{in}\\ I_L&=\frac{1-D_o}{1-2D_0}I_l\\ I_l&=\frac{V_C}{R_l}\end{aligned} \tag{2}$$

$$G_{vd}(s)=\frac{(-2I_L+I_l)L_lLs^2+[(-2I_L+I_l)R_lL+(1-D_0)(2V_C-V_{in})L+(1-2D_0)(2V_c-V_{in})L_l]s+(1-2D_0)(2V_c-V_{in})R_l}{L_lLCs^3+R_lLCs^2+[2L(1-D_0)^2+L_l(2D_0-1)^2]s+R_l(2D_0-1)^2} \quad (3)$$

$$G_{id}(s)=\frac{(2V_C-V_{in})L_lCs^2+[R_lC(2V_C-V_{in})+(1-2D_0)(-2I_L+I_l)L_l]s+(1-D_0)(2V_C-V_{in})+(1-2D_0)(-2I_L+I_l)R_l}{L_lLCs^3+R_lLCs^2+[2L(1-D_0)^2+L_l(2D_0-1)^2]s+R_l(2D_0-1)^2} \quad (4)$$

Predicting the right half plane (RHP) zeros of the related transfer functions is one of the major advantages of the small-signal modeling. By considering the control to capacitor voltage transfer function, given by Eq. 3 as an example, the numerator is a quadratic equation. As known, for a quadratic equation $ax^2+bx+c=0$, there will be two different poles α and β if the discriminant $b^2-4ac>0$. Regarding this case, it can be acquired that $a=(-2I_L+I_l)L_lL<0$ and $c=(1-2D_0)(2V_c-V_{in})R_l>0$, therefore, this transfer function has two zeros: one is negative while the other is a positive one, which is called RHP zero. This identifies a non-minimum phase characteristic in the capacitor voltage response that is known to potentially introduce stability issues in the closed loop controlled system. The design of a feedback controller with an adequate phase margin becomes more difficult when RHP zeros appear in the transfer function, since it tends to destabilize the wide bandwidth feedback loops, implying high gain instability and imposing control limitations.

3. Review of PWM control methods for ZSI

3.1. Simple ST Boost Control (SBC)

The SBC method [2], uses two straight lines equal to or greater than the peak value of the three phase references to control the ST duty ratio in a traditional sinusoidal PWM, as shown in Figure 4. When the triangular waveform is greater than the upper line, V_p, or lower than the bottom line, V_n, the circuit turns into ST state. Otherwise it operates just as traditional carrier based PWM. This method is very straightforward; however, the resulting voltage stress across the switches is relatively high because some traditional zero states are not utilized.

3.2. Maximum ST Boost Control (MBC)

Reducing the voltage stress under a desired voltage gain becomes more important to control the ZSI; this can be achieved by making the ST duty ratio as large as possible. The MBC control, [4], turns all the traditional zero states into ST state. As shown in Figure 5, the circuit is in ST state when the triangular carrier wave is either greater than the maximum curve of the references (V_a, V_b and V_c) or smaller than the minimum of the references. The ST duty ratio varies at six times of the output frequency. The ripples in the ST duty ratio will result in ripple in the inductor current and the capacitor voltage. This will cause a higher requirement of the passive components when the output frequency becomes very low. Therefore, the MBC method is suitable for applications that have a fixed or relatively high output frequency.

http://dx.doi.org/10.5772/52724

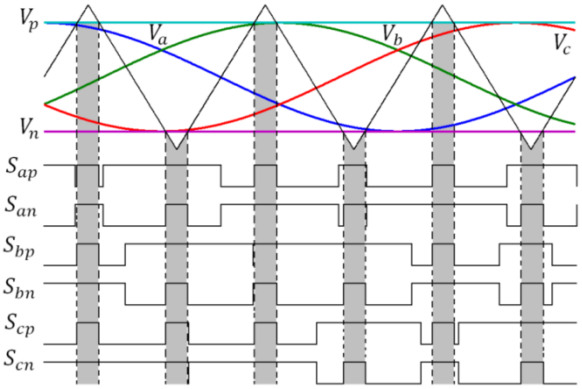

Figure 4. SBC method waveforms

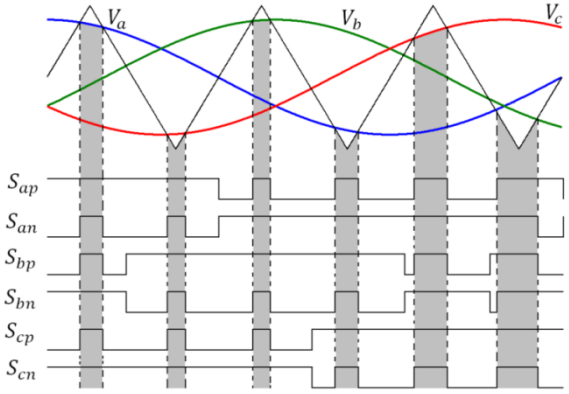

Figure 5. Waveforms of MBC method

3.3. Maximum Constant ST Boost Control (MCBC)

In order to reduce the volume and the cost, it is important always to keep the ST duty ratio constant. At the same time, a greater voltage boost for any given modulation index is desired to reduce the voltage stress across the switches. The MCBC method achieves the maximum voltage gain while always keeping the ST duty ratio constant [5]. Figure 6 shows the sketch map of the maximum constant ST boost control with third harmonic injection. Using the third harmonic injection, only two straight lines, V_p and V_n, are needed to control the ST time with 1/6 of the third harmonic injected.

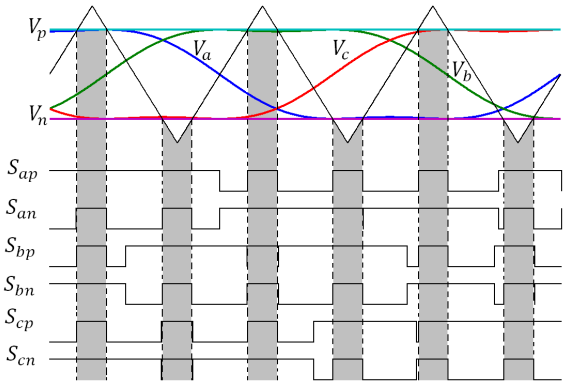

Figure 6. MCBC method with third harmonic injection

3.4. Modified Space Vector Modulation ST Control Method

The space vector PWM (SVPWM) techniques are widely used in industrial applications of the PWM inverter because of lower current harmonics and a higher modulation index. The SVPWM is suitable to control the ZSI. Unlike the traditional SVPWM, the modified space vector modulation (MSVM) has an additional ST time T_0 for boosting the dc-link voltage of the inverter beside the time intervals T_1, T_2 and T_z. The ST states are evenly assigned to each phase with $T_0/6$ within zero voltage period T_z. The zero voltage period should be diminished for generating a ST time, and the active states T_1 and T_2 are unchanged. So, the ST time does not affect the PWM control of the inverter, and it is limited to the zero state time T_z. The MSVM can be applied using two patterns. The MSVM1 as shown in Figure 7-a, at this switch pattern, the ST time T_0 is limited to $(3/4)T_z$, because the period $(T_z/4\text{-}2T_s)$ should be greater than zero. The MSVM2 as shown in Figure 7-b, where the distribution of zero state time is changed into $(T_z/6)$ and $(T_z/3)$. The maximum ST time is increased to the zero state time T_z [6].

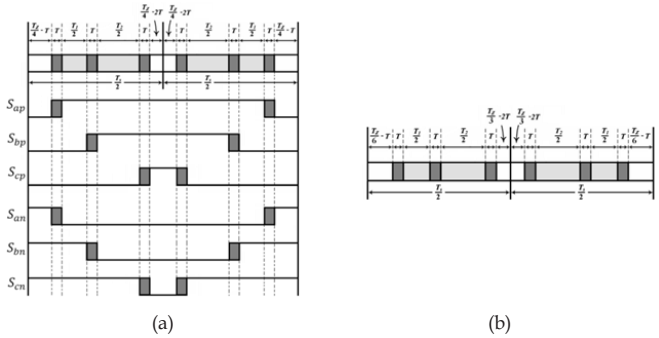

Figure 7. Switching pattern for the MSVPWM: (a) MSVM1, (b) MSVM2

http://dx.doi.org/10.5772/52724

Table 1 shows a summary of all relations for the different ST boost control methods, where D_0 is the ST duty ratio, M is the modulation index, B is the boost factor, G is the voltage gain, and Vs is the voltage stress across the switch. Figure 8-a shows the voltage gain versus the modulation index and Figure 8-b shows the voltage stress versus the voltage gain for different ST boost control methods. At high voltage gain, the MSVPWM1 has the highest voltage stress.

ST method	SBC	MBC	MCBC	MSVM1	MSVM2
D_0	$1-M$	$\frac{2\pi-3\sqrt{3}M}{2\pi}$	$\frac{2-\sqrt{3}M}{2}$	$\frac{3}{4}\cdot\frac{2\pi-3\sqrt{3}M}{2\pi}$	$\frac{2\pi-3\sqrt{3}M}{2\pi}$
B	$\frac{1}{2M-1}$	$\frac{\pi}{3\sqrt{3}M-\pi}$	$\frac{1}{\sqrt{3}M-1}$	$\frac{4\pi}{9\sqrt{3}M-2\pi}$	$\frac{\pi}{3\sqrt{3}M-\pi}$
G	$\frac{M}{2M-1}$	$\frac{\pi M}{3\sqrt{3}M-\pi}$	$\frac{M}{\sqrt{3}M-1}$	$\frac{4\pi M}{9\sqrt{3}M-2\pi}$	$\frac{\pi M}{3\sqrt{3}M-\pi}$
$M_{\max}$	$\frac{G}{2G-1}$	$\frac{\pi G}{3\sqrt{3}G-\pi}$	$\frac{G}{\sqrt{3}G-1}$	$\frac{2\pi G}{9\sqrt{3}G-4\pi}$	$\frac{\pi G}{3\sqrt{3}G-\pi}$
V_s	$(2G-1)V_{in}$	$\frac{3\sqrt{3}G-\pi}{\pi}V_{in}$	$(\sqrt{3}G-1)V_{in}$	$\frac{(9\sqrt{3}G-4\pi)}{2\pi}V_{in}$	$\frac{(3\sqrt{3}G-\pi)}{\pi}V_{in}$

Table 1. Summary of the different ST boost control methods expressions [7]

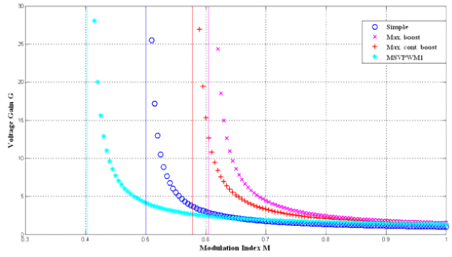

(a)

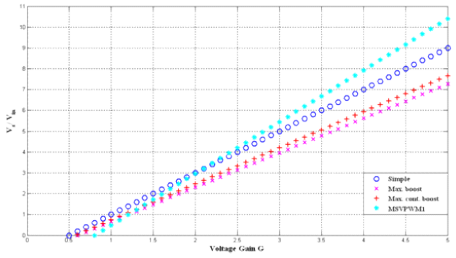

(b)

Figure 8. a) Voltage gain versus modulation index, (b) Voltage stress versus voltage gain for different PWM control methods

Efficiency evaluation is an important task during inverter design. The losses of the inverter mainly distributed on the semiconductor devices. The semiconductor device losses mainly include conduction losses and switching losses. The efficiency of the ZSI is greatly affected by the ST control methods. Figure 9 shows the losses distribution of a 10 kW ZSI at nominal input and output power, where the input diode conduction and switching losses are included, which are neglected in most publications, the extra losses of the MSVM boost method mainly come from the switching losses of IGBTs and reverse recovery losses of the input diode which are about three times of other methods [8]. Table 2 presents a comparison between the different four ST control methods. The comparison results show that the MCBC method seems to be the most suitable boost control method for the ZSI [8].

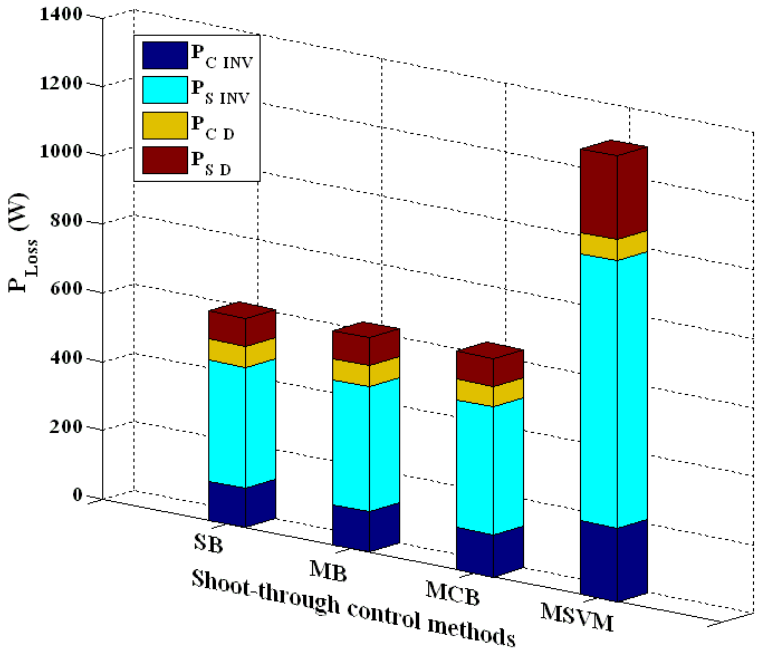

Figure 9. Losses distribution of the ZSI at 10 kW output power [8]

4. ZSI DC link voltage control

The control strategy of the ZSI is an important issue and several feedback control strategies have been investigated in recent publications [12][23]. There are four methods for controlling the ZSI dc-link voltage, which are: capacitor voltage control [12]-[19], indirect dc-link voltage control [19],[20], direct dc-link control [21],[22] and unified control [23]. Table 3, presents a review of the above mentioned control methods with their drawbacks.

http://dx.doi.org/10.5772/52724

ST boost control method	SBC	MBC	MCBC	MSVM
Line voltage harmonic	-	+	0	+
Phase current harmonic	0	0	+	-
DC link voltage ripples	0	-	+	0
Switch voltage stress	0	+	0	-
Inductor current ripples	0	-	+	-
Efficiency	0	+	+	-
Obtainable ac voltage	0	0	+	-
Total	-	+++--	+++++	+----

*(+, 0 and -) represents the best, the moderate and the lowest performance, respectively

Table 2. Different ST control methods comparison [8]

Reference No.	Control method	Controller type	Controller variable	Drawbacks
[12]	V_c control	Single loop control with a PID controller	D_0	The controller is designed based on a second order model
[13]	V_c control	Single loop control with a PI controller	D_0	The controller parameters is tuned by neural network (NN)
[15]	V_c control	Two control loops with a PI controller	D_0 and M	The controller is not designed or tuned by NN
[17], [18]	V_c control	Single loop nonlinear control	D_0 and M	Complex control algorithm
[19]	Indirect V_i control by controlling V_c	PID fuzzy controller	D_0	The controller is not accurate, because the relation between V_c and V_i is not linear and the controller is not designed
[20]	Indirect V_i control by controlling V_{ac}	PI controller with saturation	M	The ST is not controlled and the controller is not designed
[21]	Direct V_i control	Single loop PID controller	D_0	External complex sensing circuit and the controller is not designed
[22]	Direct V_i control	Dual loop V_i control, the outer voltage loop has a PI controller and the inner current loop has a P controller	D_0	A simplified representation of the 3-phase load of the ZSI
[23]	Unified control	Single loop with a PI controller	V_{ref} for the MSVM	Suitable for isolated operations and the controller is not designed

Table 3. Review of previous ZSI control strategies

In all the above mentioned control methods, a single-loop voltage control technique was used. However, in high power converters, a single-loop voltage control has two problems. The first problem is that, the inductor current is not regulated and can be overloaded during transient events and the limited stability limits is the second problem. Therefore, a dual-loop voltage control is preferred over a single-loop voltage control in high power converters to overcome the above mentioned problems [24]. Two new control algorithms are proposed by the authors, which are: a dual-loop capacitor voltage control [25] and a dual-loop peak DC-link voltage control [26]. These two control algorithms will be briefly presented as flows.

4.1. Capacitor voltage control

This chapter proposes a dual loop capacitor voltage control of the ZSI. The proposed control generates the ST duty ratio by controlling both the inductor current and the capacitor voltage of the ZSI as shown in Figure 10-a, where $G_M(s)$ is expressed by:

$$G_M(s) = \frac{D_0(s)}{v'_m(s)} = \frac{2}{V_{tri}} \tag{5}$$

Based on the small signal transfer functions $G_{vd}(s)$, $G_{id}(s)$ and $G_M(s)$ given by Eqs (3), (4) and (5), both controller transfer functions $G_{cv}(s)$ and $G_{ci}(s)$ can be designed. In order to design these controllers, the continuous time transfers functions are first discretized using the zero order hold (ZOH). Once the discrete transfer functions of the system are available, the digital controllers are designed directly in the Z-domain using methods similar to the continuous time frequency response methods. This has the advantage that the poles and zeros of the digital controllers are located directly in the Z-domain, resulting in a better load transient response, as well as better phase margin and bandwidth for the closed loop power converter [25]. Figure 10-b shows the entire digital closed loop control system containing the voltage loop controller, current loop controller, the zero order hold, the computational delay, the modified modulation, and the control to outputs transfer functions. In this implementation the chosen sampling scheme results in a computation delay of half the sampling period. The loop gains for inner current loop and outer voltage loop can be expressed as:

$$T_i(z) = G_{ci}(z) \cdot G_{id}(z) \tag{6}$$

$$T_v(z) = \frac{G_{cv}(z) \cdot G_{ci}(z) \cdot G_{vd}(z)}{1 + T_i(z)} \tag{7}$$

Where

$$G_{id}(z) = Z\left\{\frac{1 - e^{-T_s s}}{s} \cdot e^{-T_d s} \cdot G_M(s) \cdot G_{id}(s)\right\} \tag{8}$$

http://dx.doi.org/10.5772/52724

$$G_{vd}(z) = Z\left\{\frac{1-e^{-T_s s}}{s}\cdot e^{-T_d s}\cdot G_M(s)\cdot G_{vd}(s)\right\} \tag{9}$$

In this chapter, a digital PI controller with anti-windup is designed based on the required phase margin, and critical frequency, using the bode diagram of the system in the Z- domain, the transfer function of the digital PI controller in Z-domain is given by:

$$G_c(z) = K_p + \frac{K_i T_s z}{z-1} \tag{10}$$

where

$$K_p = \frac{\cos\theta}{\left|G_p(z)\right|} \tag{11}$$

$$K_i = \frac{\sin\theta\cdot f_{cz}}{\left|G_p(z)\right|} \tag{12}$$

and

$$\theta = 180^{\circ} + \phi_m - \angle G_p(z) \tag{13}$$

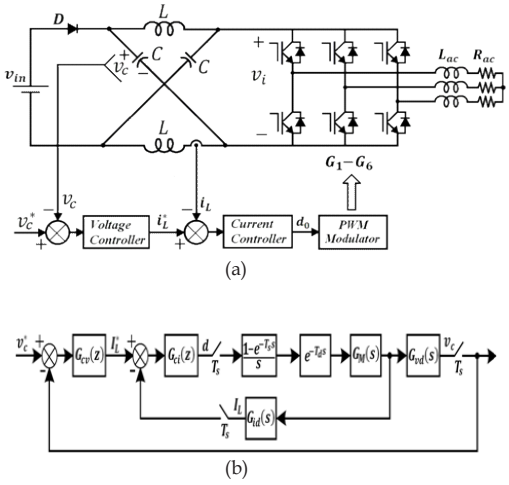

Figure 10. Dual-loop capacitor control of the ZSI (a) and its block digital block diagram (b)

Figure 11 shows the bode plots for the current loop gain and voltage loop gain, respectively, with the system parameters listed in Table 4. The plots indicate that the current loop gain has a crossover frequency as high as 1 kHz, with a phase margin of 65° and a gain margin of 10 dB. To avoid interaction between the sub-systems, low control bandwidth is used for the voltage loop. The resulting outer voltage loop has a crossover frequency of 100 Hz and a phase margin of 59° and a gain margin of 25 dB. Figs. 12-13 compare simulation and experimental results during input voltage step down by 7.5% with the same load, load increasing and decreasing by 50% and steady state operations. It is noticeable that the experimental results match the simulation results very well, which verify the performance of the proposed dual-loop capacitor voltage control for the ZSI.

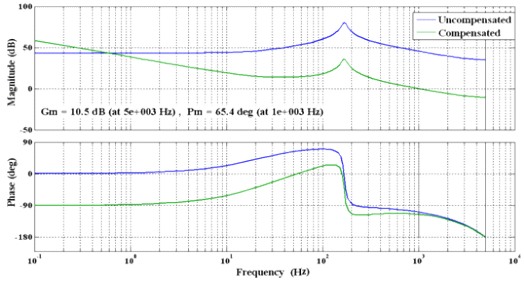

(a)

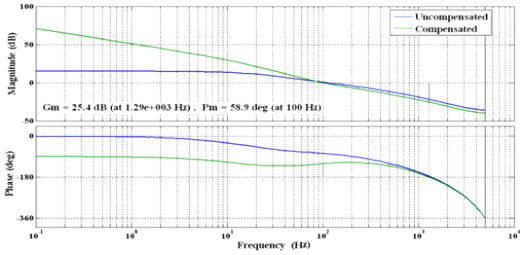

(b)

Figure 11. Bode diagrams for current (a) and voltage (b) loops for dual-loop capacitor voltage control

http://dx.doi.org/10.5772/52724

Parameter	Value
Input voltage	200 V
Capacitor reference voltage	300 V
Inductance	650 µH
Inductance internal resistance	0.22 Ω
Capacitance	320 µF
Capacitance internal resistance	0.9 mΩ
Switching frequency	10 kHz
AC load inductance	340 µH
AC load resistance	12.5 Ω

Table 4. Experimental Parameters of the ZSI

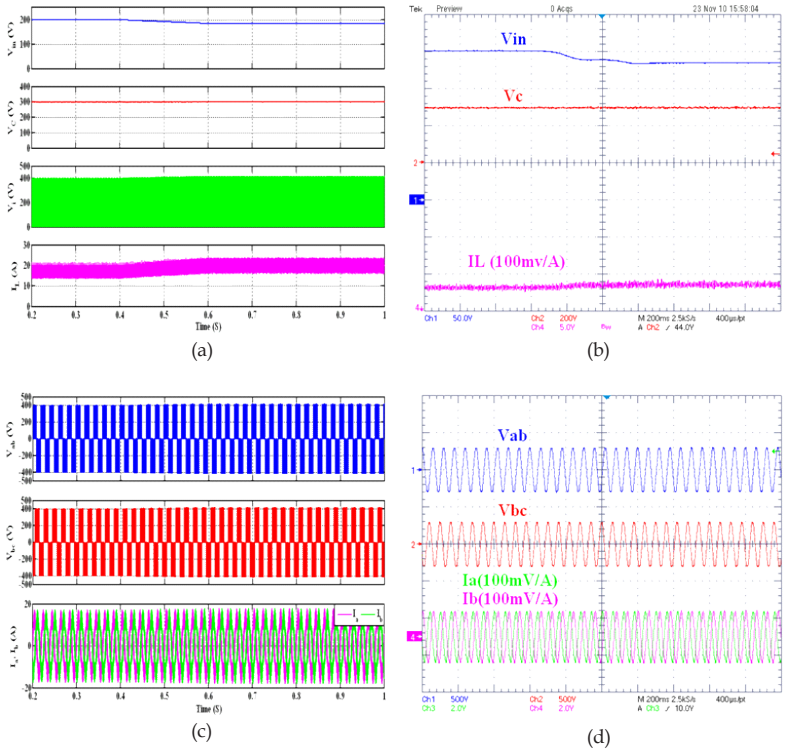

Figure 12. ZSI response during input voltage step down by 7.5% : (a and c) simulation results and (b and d) experimental results using dual-loop control technique

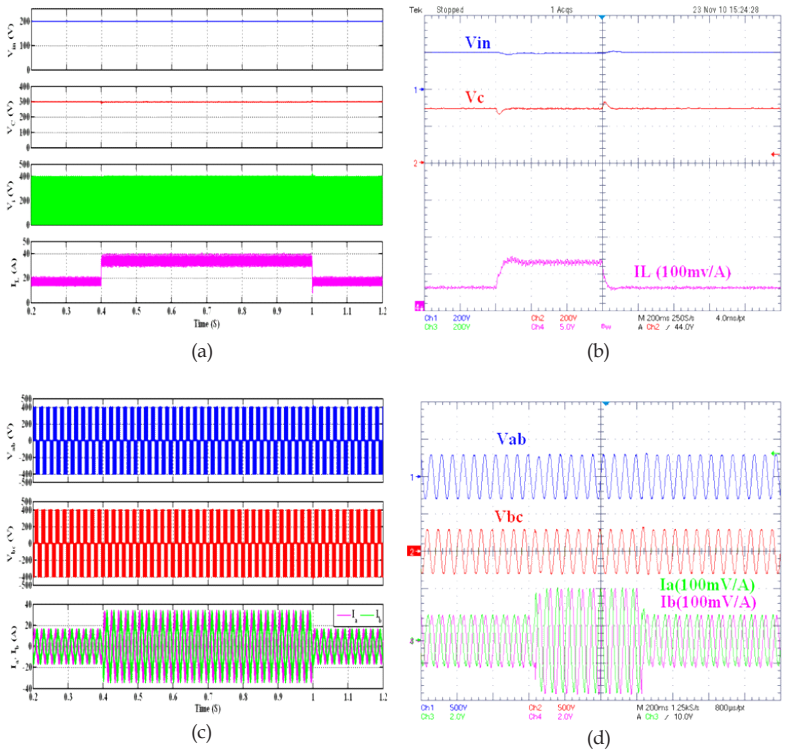

Figure 13. ZSI response during load increasing and decreasing by 50 % : (a and c) simulation results and (b and d) experimental results

4.2. Peak DC-link voltage control

The capacitor voltage, V_c, is somewhat equivalent to the peak dc-link voltage, V_{ip}, of the inverter, but the peak dc-link voltage is non-linear function of the capacitor voltage. Thus, only controlling the capacitor voltage cannot bring the high performance due to the non-linear property of the V_{ip}/V_c relation. Figure 14 shows the entire dual-loop peak dc-link voltage control technique block diagram of the ZSI. Figs. 15-16 show the simulation and experimental results of the proposed dual-loop peak dc-link voltage control technique during input voltage step and load transient. As shown in Figure 15, the input voltage stepped-down by 7.5% with the rated load, the peak dc-link voltage remains constant at 300 V, the load phase current and line voltage are not affected by input voltage decreasing and the inductor current is increased to supply the same output power. Figure 16 shows the ZSI response during load increasing and decreasing by 50%. As noticeable the inductor current is doubled during the 50% load increase and the output line voltage and the peak dc-link voltage remain unchanged.

http://dx.doi.org/10.5772/52724

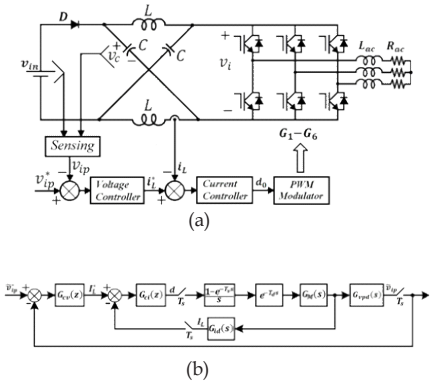

Figure 14. ZSI dual loop peak dc-link voltage control of the ZST (a) and its block diagram (b)

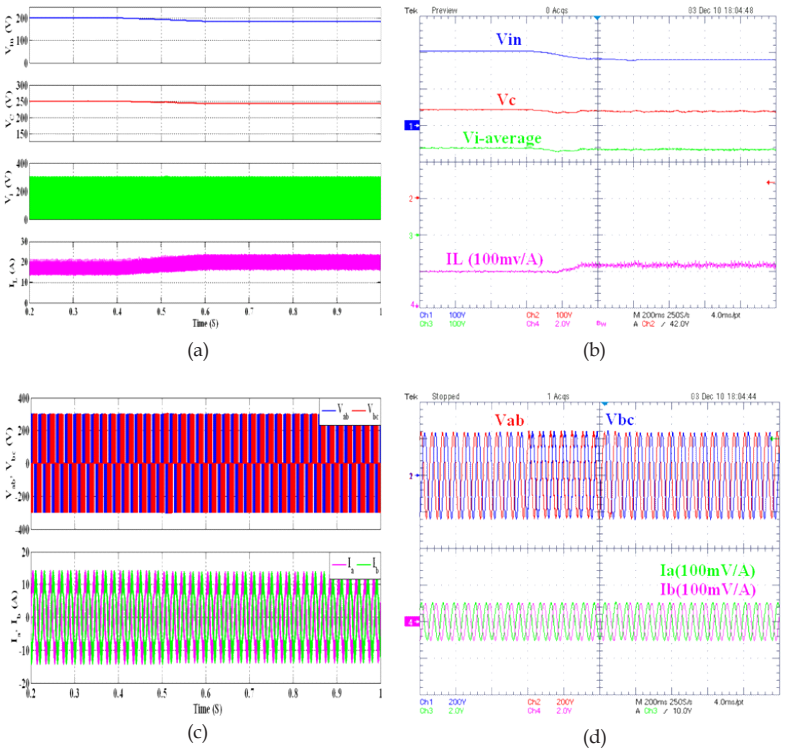

Figure 15. ZSI response during input voltage step down by 7.5%: (a, b) Z-network variables and (c, d) output variables

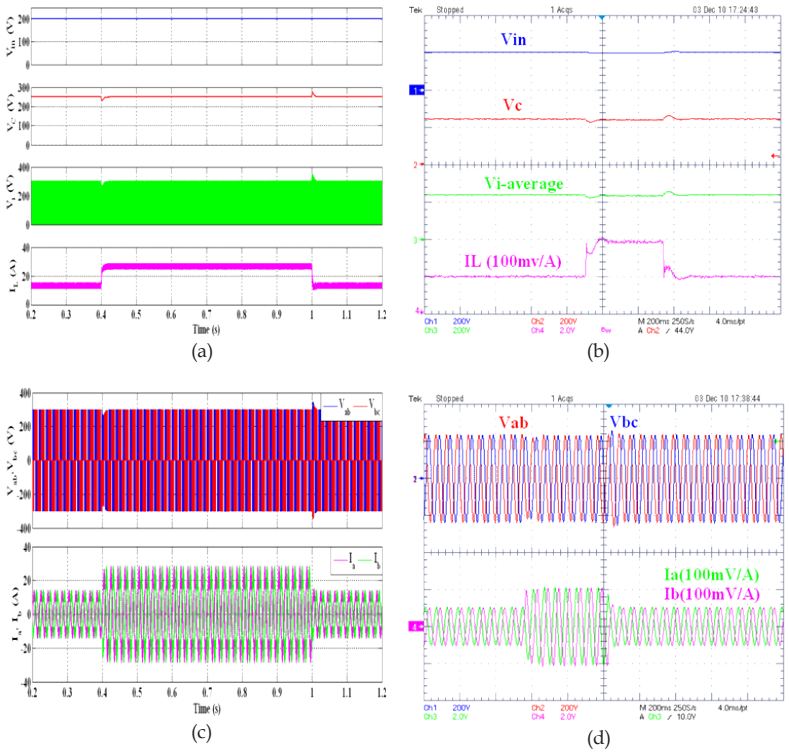

Figure 16. ZSI response during input voltage step down by 7.5% : (a, b) Z-network variables and (c, d) output variables

5. A comparative study of different control techniques for induction motor fed by a Z-source inverter

This section presents a comparative study of the most significant control methods (Scalar control (V/F), indirect field oriented control (IFOC) and direct torque control (DTC)) for an induction motor fed by a ZSI for automotive applications. The three control techniques are implemented using PWM voltage modulation. The comparison is based on various criteria including: basic control characteristics, dynamic performance, and implementation complexity. The study is done by MATLAB simulation of a 15 kW induction motor fed by a high performance ZSI (HP-ZSI). The simulation results indicates that, the IFOC seems to be the best control techniques suitable for controlling an induction motor fed by a ZSI for automotive applications.

http://dx.doi.org/10.5772/52724

5.1. Scalar control (V/F) technique

The closed loop speed control by slip regulation, which is an improvement of the open loop V/F control, is shown in Figure 17. The speed loop error generates the slip command ω_{sl}^* through a proportional integral (PI) controller with a limiter. The slip is added to the feedback speed signal to generate the slip frequency commandω_e^*. Thus the frequency command generates the voltage command through a V/F generator, which incorporates the low frequency stator drop compensation. Although this control technique is simple, it provides limited speed accuracy especially in the low speed range and poor dynamic torque response.

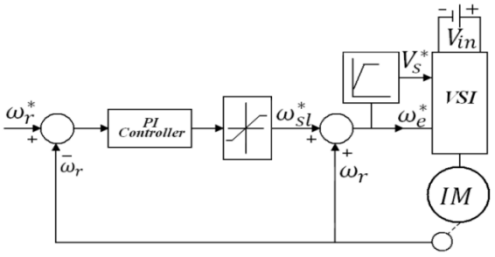

Figure 17. Block diagram of a scalar controlled induction motor

5.2. Indirect Field Oriented Control (IFOC) technique

In the indirect field oriented control method, the rotating reference frame is rotating at synchronous angular velocity, ω_e. This reference frame allows the three phase currents to be viewed as two dc quantities under steady state conditions. The q-axis component is responsible for the torque producing current, i_{qs}, and the d-axis is responsible for the field producing current, i_{ds}. These two vectors are orthogonal to each other so that the field current and the torque current can be controlled independently. Figure 18 shows the block diagram of the IFOC technique for an induction motor. The q-axis component of the stator reference current, i_{qs}^*, may be computed using the reference torque, T_{ref}, which is the output of a PI speed controller, as:

$$i_{qs}^* = \frac{2}{3}\frac{2}{p}\frac{L_r}{L_m}\frac{T_{ref}}{\psi_r} \tag{14}$$

where Ψ_r is the estimated rotor flux, which is given by:

$$\psi_r = \frac{L_m}{\tau_r s + 1} i_{ds} \tag{15}$$

where L_m, L_r and τ_r are the magnetization inductance, the rotor inductance, and the rotor time constant, respectively. The d-axis component of the stator reference current, i_{ds}^*, may also be obtained by using the reference input flux, $\psi_{r_{ref}}$, which is the output of a PI flux controller, as:

$$i_{ds}^* = \frac{\psi_{r_{ref}}}{L_m} \tag{16}$$

By using the rotor speed, ω_{rm}, and the slip frequency, ω_{sl}, which is given by:

$$\omega_{sl} = \frac{1}{\tau_r} \frac{i_{ds}^*}{i_{qs}^*} \tag{17}$$

the angle of the rotor flux, θ_e, may be evaluated as:

$$\theta_e = \int (\omega_e + \omega_{rm}) dt \tag{18}$$

Proportional integral controllers regulate the stator voltages, v_{ds}^* and v_{qs}^*, to achieve the calculated reference stator currents, i_{ds}^* and i_{qs}^*. The required voltage is then synthesized by the inverter using pulse width modulation (PWM). During motor operation the actual rotor resistance and inductance can vary. The resulting errors between the values used and the actual parameters cause an incomplete decoupling between the torque and the flux. In order to compensate for this incomplete decoupling, the values of compensation voltages are added to the output of the current controllers. This voltage compensation can improve the performance of the current control loops. The compensations terms are given by:

$$\begin{aligned} v_{dsc} &= -\omega_e \sigma L_s i_{qs}^* \\ v_{dsc} &= \omega_e \sigma L_s i_{ds}^* + \frac{L_m}{L_r} \omega_r \psi_r \end{aligned} \tag{19}$$

5.3. Direct Torque Control with Space Vector Modulation (DTC-SVM) technique

The conventional DTC scheme has many drawbacks, such as: variable switching frequency, high current and torque ripples, starting and low-speed operation problems, in addition to

http://dx.doi.org/10.5772/52724

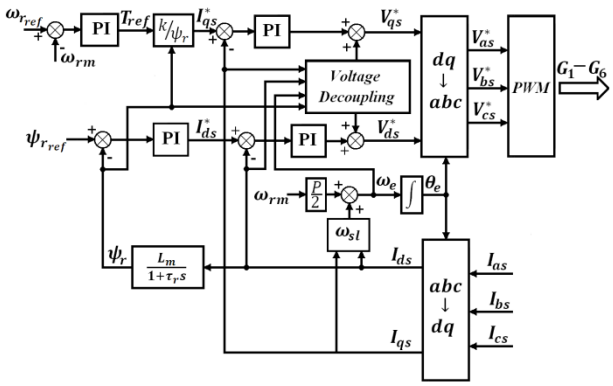

Figure 18. Block diagram of the IFOC of an induction motor

high sampling frequency needed for digital implementation of the hysteresis controllers. To overcome these drawbacks, the space vector modulation is combined with the conventional DTC scheme for induction motor drive to provide a constant inverter switching frequency. In the DTC-SVM scheme, as shown in Figure 19, the torque and flux hysteresis comparators are replaced by PI controllers to regulate the flux and torque magnitudes respectively. The motor stator flux and the motor developed torque can be estimated by:

$$\begin{aligned}
\psi_{ds} &= \int \left(v_{ds} - R_s i_{ds} \right) dt \\
\psi_{qs} &= \int \left(v_{qs} - R_s i_{qs} \right) dt \\
\left| \psi_s \right| &= \sqrt{\psi_{ds}^2 + \psi_{ds}^2} \\
\theta_{\psi_s} &= \tan^{-1} \frac{\psi_{qs}}{\psi_{ds}}
\end{aligned} \tag{20}$$

$$T_e = \frac{3}{2} P \left(\psi_{ds} i_{qs} - \psi_{qs} i_{ds} \right) \tag{21}$$

The output of theses PI controllers generates the d and q components of the reference voltage command (v_{ds}^* and v_{qs}^*) in the stator flux oriented coordinates. After coordinate transformation, using the stator flux angle $\theta_{\psi s}$, we get the reference voltage vectors $v_{\alpha s}^*$ and $v_{\beta s}^*$) in the stationary frame. These two components, which can control stator flux and torque separately, are delivered to space vector modulator (SVM). The space vector modulator generates the inverter control signals, which ensures fixed inverter switching frequency. So the inverter switching frequency is significantly increased, and the associated torque ripple and current harmonics can be dramatically reduced, in comparison with the conventional switching table based DTC scheme.

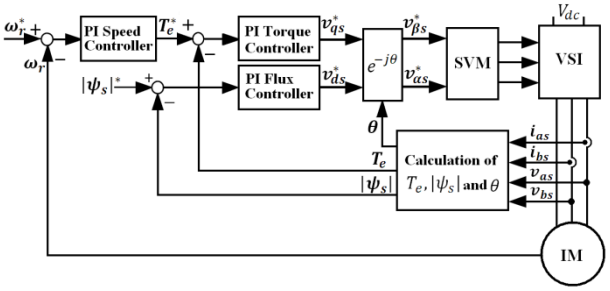

Figure 19. Block diagram of the DTC-SVM based IM drive

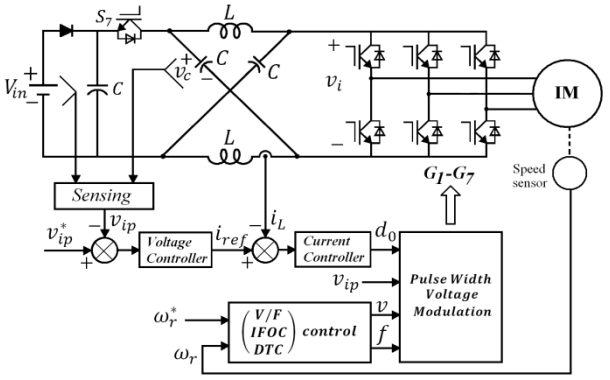

Figure 20. Closed loop speed control of three phase induction motor fed by a high performance ZSI

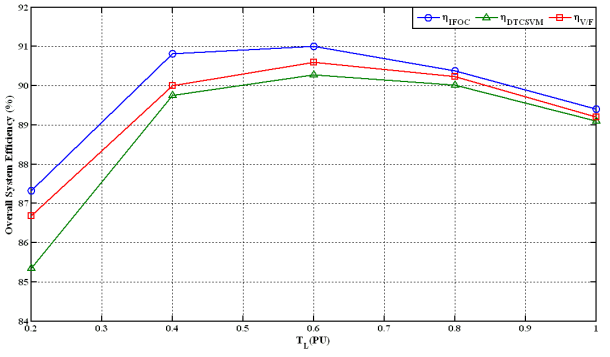

Figure 21. Overall system efficiency at different load torque values

Figure 20 shows the complete block diagram of the closed loop speed controlled IM fed by a high performance ZSI. A dual loop controller is designed to control the average value of the dc link voltage by controlling the magnitude of its peak voltage based on a small signal model of the high performance ZSI. Figure 21, shows the calculated overall system efficiency at different load torque. The three control techniques were compared on a simulated benchmark. The main results of this comparative study are summarized in Table 5.

Comparison Criterion	V/F	IFOC	DTC-SVM
Dynamic response	Poor	Good	Good
Torque ripples	Large	Small	Small
Speed error	Large	Small	Medium
ZSI performance	Good	Good	Poor
Complexity	Low	High	High
Efficiency	Medium	High	Low

Table 5. Summary of performance compression

6. Z-Source Inverter for vehicular applications

This section proposes three applications of the ZSI in the automotive field. The first application proposes the using of the bidirectional ZSI (BZSI) supplied by a battery to drive an induction motor for hybrid electric vehicle (HEV) applications, by replacing the two stages conversion. The second application proposes the using of the BZSI in plug-in hybrid electric vehicle (PHEV) applications for replacing the bidirectional battery charger, which composed of two stages conversion. By using the BSZI, the battery can be charged from the grid during night and can be discharged to the grid during peak power demand, which increase the grid stability. The third application proposes the using of the HP-ZSI for fuel cell hybrid electric vehicle (FCHEV) applications. Where the fuel cell (FC) stack and the supercapacitor (SC) module are directly connected in parallel with the HP-ZSI. The SC module is connected between the input diode and the bidirectional switch S_7 of the HP-ZSI. The SC module supplies the transient and instantaneous peak power demands and absorbs the deceleration and regenerative braking energy. The indirect field oriented control (IFOC) is used to control the speed of the IM during motoring and regenerative braking operation modes in the first and the third proposed applications. While, a proportional plus resonance (PR) controller is used to control the AC current during connecting the BZSI to the grid for battery charging/discharging mode in the second proposed application.

6.1. ZSI applications in HEV

The ZSI is proposed to be used to replace the two stages conversion in HEV, The BZSI can replace the bidirectional DC/DC converter and the traditional VSI as a single stage convert-

er, as shown in Figure 22. The IFOC is used for controlling the speed of the IM during motoring and regenerative braking operations and a dual loop capacitor voltage control algorithm is used to control the BZSI dc-link voltage.

6.2. ZSI applications in PHEV

The ZSI is proposed to be used to replace the two stage bidirectional battery charger in a PHEV. Figure 23 shows the entire block diagram of a grid connected BZSI containing: the battery, the BZSI, the capacitor voltage control algorithm and the AC grid current control algorithm during battery charging/discharging modes, where the capacitor voltage control generates the ST duty ratio and the AC grid current control generates the modulation index.

6.3. ZSI applications in FCHEV

In Figure 24, the FC system and the SC module are direct connected in parallel with the HP-ZSI. The SC module is connected between the input diode D and the bidirectional switch S_7. The bidirectional switch S_7 provides a path for the regenerative braking energy to be stored in the SC module during the ST state. The SC module supplies the transient and instantaneous peak power demands and absorbs the deceleration and regenerative braking energy. In addition, a dual loop control is used to control the Z-network capacitor voltage by controlling the ST duty ratio and the IFOC strategy is used to control the induction motor speed by controlling the modulation index. The proposed applications improve the vehicle efficiency and reduce its production cost due to a lower its component count, since it is a one stage converter with a reduced volume and easier control algorithm.

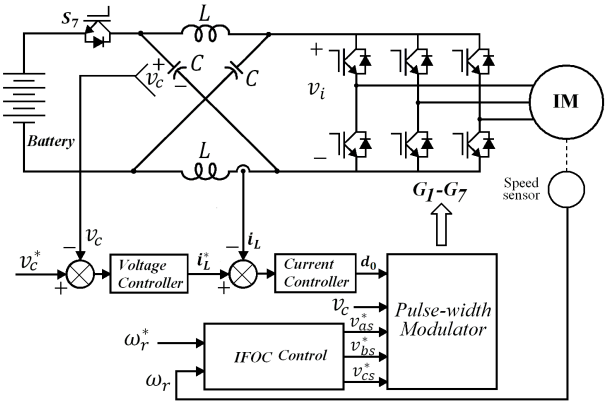

Figure 22. Using the BZSI for HEV applications

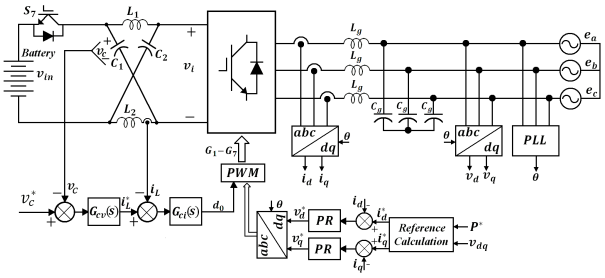

Figure 23. Using the BZSI for PHEV applications

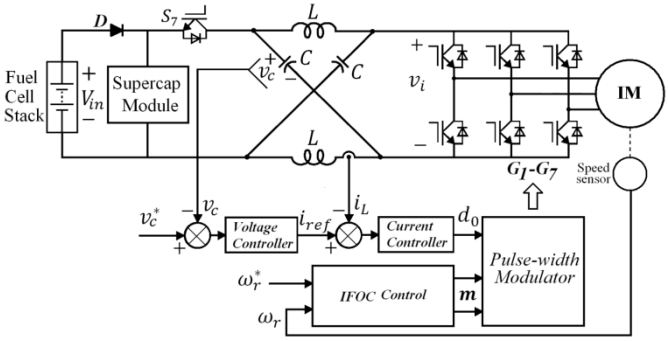

Figure 24. Using the HP-ZSI for FCHEV applications

Author details

Omar Ellabban[1*] and Joeri Van Mierlo[2*]

1 Department of Power and Electrical Machines, Faculty of Engineering, Helwan University, Cairo, Egypt

2 Department of Electric Engineering and Energy Technology, Faculty of Engineering Sciences, Vrije Universiteit Brussel, Brussels, Belgium

References

[1] Emadi, A., Young, Joo., & Lee, Rajashekara. K. (2008). Power Electronics and Motor Drives in Electric, Hybrid Electric, and Plug-In Hybrid Electric Vehicles. *IEEE Transactions on Industrial Electronics.*, 55(6), 2237-2245.

[2] Peng, FZ. (2003). Z-source Inverter. *IEEE Transactions on Industry Applications*, 39(2), 504-510.

[3] Peng, F. Z., Shen, M., & Joseph, A. (2005). Z-Source Inverters, Controls, and Motor Drive Applications. *KIEE International Transactions on Electrical Machinery and Energy Conversion Systems*., 5, 6-12.

[4] Peng, F. Z., Shen, M., & Qian, Z. (2005). Maximum boost control of the Z-source inverter. *IEEE Transactions on Power Electronic*., 20(4), 833-838.

[5] Shen, M., Wang, J., Joseph, A., Peng, F. Z., Tolbert, L. M., & Adams, D. J. (2006). Constant boost control of the Z-source inverter to minimize current ripple and voltage stress. *IEEE Transactions on Industry Applications*, 42(3), 770-778.

[6] Poh, Chiang., Loh, D., Mahinda, Vilathgamuwa., Yue, Sen., Lai, Geok., Tin, Chua., & Yunwei, Li. (2005). Pulse-Width Modulation of Z-Source Inverters. *IEEE Transactions on Power Electronics*., 20(6), 1346-1355.

[7] Ellabban, O., Van Mierlo, J., & Lataire, P. (2009). Comparison between Different Shoot-Through PWM Control Methods for Different Voltage Type Z-Source Inverter Topologies. The 13th European Conference on Power Electronics and Applications.

[8] Ellabban, O., Van Mierlo, J., & Lataire, P. (2011). Experimental Study of the Shoot-Through Boost Control Methods for the Z-Source Inverter. *EPE- European Power Electronics and Drives Journal*., 21(2), 18-29.

[9] Rajakaruna, S., & Jayawickrama, L. (2010). Steady-State Analysis and Designing Impedance Network of Z-Source Inverters. *IEEE Transactions on Industrial Electronics*, 57(7), 2483-2491.

[10] Loh PC, Vilathgamuwa DM, Gajanayake CJ, Lim YR, Teo CW. (2007). Transient Modeling and Analysis of Pulse-Width Modulated Z-source Inverter. *IEEE Transactions on Power Electronics*., 22(2), 498-507.

[11] Liu, J., Hu, J., & Xu, L. (2007). Dynamic Modeling and Analysis of Z-Source Converter-Derivation of AC Small Signal Model and Design-Oriented Analysis. *IEEE Transactions of Power Electronics*., 22(5), 1786-1796.

[12] Xinping, D., Zhaoming, Q., Shuitao, Y., Bin, C., & Fangzheng, P. (2007). A PID Control Strategy for DC-link Boost Voltage in Z-source Inverter. The Twenty Second Annual IEEE Applied Power Electronics Conference., 1145-1148.

[13] Rastegar, Fatemi., Mirzakuchaki, S., & Rastegar, Fatemi. S. M. J. (2008). Wide-Range Control of Output Voltage in Z-Source Inverter by Neural Network. The International Conference on Electrical Machines and Systems., 1653-1658.

[14] Tran QV, Chun TW, Kim HG, Nho EC,. (2009). Minimization of Voltage Stress across Switching Devices in the Z-Source Inverter by Capacitor Voltage Control. *Journal of Power Electronics*, 9(3), 335-342.

[15] Rostami, H., & Khaburi, D. A. (2010). Neural Networks Controlling for Both the DC Boost and AC Output Voltage of Z-Source Inverter. The 1st Power Electronic & Drive Systems & Technologies Conference. ., 135-140.

[16] Shen, M., Tang, Q., & Peng, F. Z. (2007). Modeling and Controller Design of the Z-Source Inverter with Inductive Load. The IEEE Power Electronics Specialists Conference., 1804-1809.

[17] Rajaei, A. H., Kaboli, S., & Emadi, A. (2008). Sliding-mode control of Z-source inverter. The 34th Annual Conference of IEEE Industrial Electronics., 947-952.

[18] Mo, W., Loh, P. C., & Blaabjerg, F. (2011). Model predictive control for Z-source power converter. The 8th International Conference on Power Electronics., 3022-3028.

[19] Ding, X., Qian, Z., Yang, S., Cui, B., & Peng, F. (2008). A Direct DC-link Boost Voltage PID-Like Fuzzy Control Strategy in Z-Source Inverter. The IEEE Power Electronics Specialists Conference., 405-411.

[20] Tang, Y., Xie, S., & Zhang, C. (2009). Feedforward plus feedback control of the improved Z-source inverter. *IEEE Energy Conversion Congress and Exposition.*, 783-788.

[21] Ding, X., Qian, Z., Yang, S., Cui, B., & Peng, F. (2007). A Direct Peak DC-link Boost Voltage Control Strategy in Z-Source Inverter. The Twenty Second Annual IEEE Applied Power Electronics Conference., 648-653.

[22] Sen, G., & Elbuluk, M. (2010). Voltage and Current Programmed Modes in Control of the Z-Source Converter. *IEEE Transactions on Industry Applications*, 46(2), 680-686.

[23] Yang, S., Ding, X., Zhang, F., Peng, F. Z., & Qian, Z. (2008). Unified Control Technique for Z-Source Inverter. The IEEE Power Electronics Specialists Conference., 3236-3242.

[24] Ellabban, O., Joeri Van, Mierlo. J., & Lataire, P. (2011). Capacitor Voltage Control Techniques of the Z-source Inverter: A Comparative Study. *EPE- European Power Electronics and Drives Journal.*, 21(4), 13-24.

[25] Ellabban, O., Joeri Van, Mierlo. J., & Lataire, P. (2011). Design and Implementation of a DSP Based Dual-Loop Capacitor Voltage Control of the Z-Source Inverter. *International Review of Electrical Engineering*, 6(1), 98-108.

[26] Ellabban, O., Joeri Van, Mierlo. J., & Lataire, P. (2012). A DSP Based Dual-Loop Peak DC-link Voltage Control of the Z-Source Inverter. *IEEE power Electronics Transactions.*, 27(9), 4088-4097.

[27] Peng, F. Z., Joseph, A., Wang, J., Shen, M., Chen, L., & Pan, Z. (2005). Z-Source Inverter for motor drives. *IEEE Transaction on power electronics.*, 20(4), 857-863.

[28] Ding, X., Qian, Z., Yang, S., Cui, B., & Peng, F. (2007). A New Adjustable-Speed Drives (ASD) System Based on High-Performance Z-Source Inverter. *IEEE Industry Applications Conference.*, 2327-2332.

[29] Ellabban, O., Van Mierlo, J., & Lataire, P. (2010). A new Closed Loop Speed Control of Induction Motor Fed by a High Performance Z-Source Inverter. The IEEE Electrical power and energy conference.

[30] Ellabban, O., Van Mierlo, J., & Lataire, P. (2011). Direct Torque Controlled Space Vector Modulated Induction Motor Fed by a Z-source Inverter for Electric Vehicles. *The III International Conference on Power Engineering, Energy and Electrical Drives.*

[31] Ellabban, O., Van Mierlo, J., & Lataire, P. (2011). A Comparative Study of Different Control Techniques for Induction Motor Fed by a Z-Source Inverter for Electric Vehicles. *The III International Conference on Power Engineering, Energy and Electrical Drives.*

[32] Peng, F. Z., Shen, M., & Holland, K. (2007). Z-source Inverter Control for Traction Drive of Fuel Cell- Battery Hybrid Vehicles. *IEEE Transactions on Power Electronics.*, 22(3), 1054-1061.

[33] Shen, M., Hodek, S., Fang, Z., & Peng, F. Z. (2007). Control of the Z-Source inverter for FCHEV with the battery connected to the motor neutral point. *IEEE Power Electronics Specialist Conference.*, 1485-1490.

[34] Dehghan, S. M., Mohamadian, M., & Yazdian, A. (2010). Hybrid electric vehicle based on bidirectional z-source nine-switch inverter. *IEEE Transactions on Vehicular Technology*, 59(6), 2641-2653.

[35] Ellabban, O., Van Mierlo, J., & Lataire, P. (2010). Control of a Bidirectional Z-Source Inverter for Hybrid Electric Vehicles in Motoring, Regenerative Braking and Grid Interface Operations. The IEEE Electrical power and energy conference.

[36] Ellabban, O., Van Mierlo, J., Lataire, P., & Hegazy, O. (2010). Control of a High-Performance Z-Source Inverter for a Fuel Cell/ Supercapacitor Hybrid Electric Vehicles. The 25th World Battery, Hybrid and Fuel Cell Electric Vehicle Symposium & Exhibition.

[37] Ellabban, O., Van Mierlo, J., & Lataire, P. (2011). Control of a Bidirectional Z-Source Inverter for Electric Vehicle Applications in Different Operation Modes. *Journal of Power Electronics*, 11(2), 120-131.